Temperature induced phase transition of CaMn0.5Zr1.5(PO4)3 phosphate

Maria Orlova, Lukas Perfler, Martina Tribus, Petr Salnikov, Benoit Glorieux, Albina Orlova

Temperature induced phase transition of $CaMn_{0.5}Zr_{1.5}(PO_4)_3$ phosphate

Maria Orlova [a,*], Lukas Perfler [a], Martina Tribus [a], Petr Salnikov [b], Benoit Glorieux [c], Albina Orlova [b]

[a] Institute of Mineralogy and Petrography, University of Innsbruck, Innrain 52, Innsbruck 6020, Austria
[b] Department of Chemistry, University of Nizhny Novgorod, 23 Gagarin Avenue, Nizhny Novgorod 603950, Russia
[c] CNRS, University of Bordeaux, ICMCB, 87 Albert Schweitzer Avenue, Pessac 33600, France

Keywords:
Phosphates
Phase transition
Crystal structure
X-ray powder diffraction
Ab-initio structure solution

A B S T R A C T

In this work we investigated the structural behaviour of a $CaMn_{0.5}Zr_{1.5}(PO_4)_3$. Due to the presence of divalent Mn^{2+} cations this compound can possess interesting luminescence properties. It was recently understood that this phosphate undergoes a temperature induced irreversible phase transition in the range of 800 875 °C. It has also been shown that the *3d 3d* luminescence of Mn^{2+} increases 10 fold for the high temperature polymorph. To determine the Mn environment structural investigations of both phases have been performed by the X ray powder diffraction and Raman spectroscopy methods. The low temperature modification adopts the trigonal *NZP* structure type with a slightly lower symmetry (space group *R*32, $a=8.7850(2)$ Å, $c=22.6496(7)$ Å, $V=1514.8(1)$ Å^3). The high temperature form in turn has orthorhombic symmetry (space group *Pnma*, $a=6.2350(3)$ Å, $b=6.6281(3)$ Å, $c=14.4731(6)$ Å, $V=598.13(5)$ Å^3). Both structures were solved *ab initio* from powder data and structural analysis was performed. *In situ* and RT Raman spectra are consistent with the XRD derived structural model. Mn^{2+} cations occupy different types of positions in these structures and a change in Mn coordination number (6 for LT phase, 7 for HT phase) results in different Mn O bond lengths. These differences may explain the change in the optical properties between the polymorphs.

1. Introduction

$NaZr_2(PO_4)_3$ *(NZP , NASICON)* type compounds belong to the large class of $Met_m(PO_4)_n$ phosphates with three dimensional framework structures [1]. Materials of this family show iso and heterovalent isomorphism properties, both in the framework of the structure and in the cavities. Due to cationic/anionic sub stitution it is possible to design compounds with interesting electrical, magnetic, and mechanical properties. Recently, these phosphates have drawn much attention due to their possible ap plication for photodiode technologies since they allow the in corporation of *d* and *f* elements which are responsible for luminescence.

Examples of these phosphates include Eu^{2+}: $Eu_{0.5}Zr_2(PO_4)_3$:Eu [2], $Ca_{0.5}Zr_2(PO_4)_3$:Eu, $Sr_{0.5}Zr_2(PO_4)_3$:Eu, $Ba_{0.5}Zr_2(PO_4)_3$:Eu [3], $Ca_{0.5\ x}Eu_xZr_2(PO_4)_3$ [4]; Eu^{3+}: $Eu_{0.33}Zr_2(PO_4)_3$ [5], $Na_3Al_2(PO_4)3$: Eu [6], $Ca_{0.5}Fe_{1\ x}Eu_xSb(PO_4)_3$ [7], $La_{1/6}Pb_{1/3}Zr_2(PO_4)_{17/6}(SiO_4)_{1/6}$:Eu [8]; Mn^{2+}: $Na_3Al_2(PO_4)_3$:Mn, $Mn_{0.5}Zr_2(PO_4)_3$:Mn [9], $Ca_{0.4}Mn_{0.1}Zr_2(PO_4)_3$ [10].

In this work we investigated the structural behaviour of a $CaMn_{0.5}Zr_{1.5}(PO_4)_3$. Due to the presence of divalent Mn^{2+} cations this compound can possess interesting optical properties. Fur thermore, it has been reported that this compound exists in two polymorphs and that luminescence properties increase drastically (about 10 times) for the high temperature polymorph [11]. In or der to obtain a better understanding of the luminescence me chanism structural investigations of the different polymorphs have been performed. Both structures were solved *ab initio* from pow der diffraction data using crystal chemical information from si milar phases. The results of this study are presented. The knowl edge obtained could be useful for developing materials with im proved optical properties.

2. Material and methods

2.1. Synthesis

$CaMn_{0.5}Zr_{1.5}(PO_4)_3$ was synthesized according to the following procedure: solutions of manganese acetate $Mn(CH_3COO)_2$ (1 M) and calcium nitrate $Ca(NO_3)_2$ (1 M) were added to a solution of zirconium oxychloride $ZrOCl_2$ (1 M), to which solutions of am monium dihydrogen phosphate $NH_4H_2PO_4$ (1 M) and ethylene glycol (1 M) were simultaneously added dropwise to under

* Corresponding author.
E-mail address: maria.p.orlova@gmail.com (M. Orlova).

vigorous continuous stirring. The resulting white gel was further stirred under the same conditions for 15 min and dried at a temperature of 130 °C until the moisture was removed (visually). The dried gel (dark brown in colour) was subsequently heated at a temperature of 380 °C for two days. The black product thus formed was annealed at temperatures of 700, 900 °C for 20 h at each stage with intermediate careful grinding manually in an agate mortar. LT phase synthesis was finished at 700 °C, HT at 900 °C. After final temperature of annealing samples were quenched.

2.2. X ray diffraction

X ray powder diffraction data at ambient conditions were collected on a STOE STADI MP diffractometer using strictly monochromatic Cu $K_{\alpha 1}$ radiation ($\lambda = 1.540593$ Å) from a focusing Ge (111) primary beam monochromator and a Mythen1k detector with 11° detection range, FWHM was equal to 0.048° at 26.56° 2θ. Data acquisition was performed in the range between 8 and 110° 2θ with a step size of 0.009°. Measurements were taken in bisecting transmission geometry, with a sample of 2 mm diameter placed between two zero scattering foils.

2.3. Raman spectroscopy

Raman spectra of the polycrystalline phosphates were recorded in the range of 50 4000 cm^{-1} with a Horiba Jobin Yvon Labram HR 800 Raman microspectrometer. The samples were excited using the 532 nm emission line of a frequency doubled 25 mW Nd:YAG laser and the 633 nm emission line of a 17 mW helium neon laser under an Olympus 100× objective lens (numerical aperture of 0.9). The size of the laser spot on the surface was approximately 1 μm in diameter. The scattered light was dispersed by an optical grating with 1800 lines mm^{-1} and collected by a 1024 × 256 open electrode CCD detector. The spectral resolution, determined by measuring the Rayleigh line, was about 2 cm^{-1}. The accuracy of the Raman line shifts, calibrated by measuring a silicon standard, was in the order of 0.5 cm^{-1}. Background and Raman bands were fitted by the built in spectrometer software LabSpec 5 to first or second order polynomials and convoluted Gaussian Lorentzian functions, respectively. The calculation of the number and symmetry of the vibrational modes were carried out using the crystallographic information file and the SAM programme [11 15] . *In situ* high temperature Raman experiments were performed on a Linkam TS1500 heating stage. The phosphate sample was loaded into the ceramic crucible on a 7 mm sapphire disc. Measurements were performed from room temperature up to 1100 °C.

2.4. Optical analysis

In order to analyse the possibility of presence of Mn^{3+} ions, photoluminescence measurement was performed using a spectrofluorimeter SPEX FL212. As mentioned by Mouline et al. [9], the presence of Mn^{3+} would be revealed by a broad emission band around 800 nm, following an excitation band at 280 nm. No band in this range appeared for the studied compound. Hence, there is no evidence of trivalent manganese in the studied samples.

2.5. EDS analysis

In order to confirm the phase composition of synthesized samples and in particular the presence of Mn cations in main phase, EDS examinations has been performed.

EDX data were acquired using a scanning electron microscope (JEOL JSM6010 LV) and a Bruker QUANTAX system equipped with a peltier cooled BRUKER XFlash 410 M silicon drift detector. The powder was placed on double sided sticky carbon tape and coated with a thin conductive carbon layer. The operating conditions for EDX analysis were as follows: 15 kV accelerating voltage, 13.5 mm working distance, 2900 cps output count rate, 60 s livetime, 2% deadtime. Semi quantitative (standardless) results were based on a peak to background ZAF evaluation method (P/B ZAF) and a series fit deconvolution model provided by the Esprit 1.9 software (Bruker). Due to the standardless method, the totals are normalized to 100%. Semi quantitaive analysis gives an atomic ratio of 5.66 at% Ca, 2.80 at% Mn, 11.18 at% Zr, 12.31 at% P and 68.05 at% O resulting in a chemical formula of $Ca_{1.02}Mn_{0.50}Zr_{2.01}P_{2.22}O_{12.25}$. A source of uncertainty in P and Zr content can be found in a strong peak overlap between P K series (2.014 2.142 keV) and Zr L series (1.792 2.547 keV).

2.6. Structure solution and refinement

$CaMn_{0.5}Zr_{1.5}(PO_4)_3$ phosphate synthesized at 700 °C (LT modification) adopts a trigonal *R* centred unit cell similar to that of $NaZr_2(PO_4)_3$ (*R* 3*c*). However, two weak reflections at 11.65 and 12.24° 2θ (*Miller indices* (*003*) *and* (*101*)), respectively, violate the extinction rule of the *c* glide plane. Under the assumption of trigonal symmetry the following five possible space groups remain: *R*3, *R* 3, *R*32, *R*3*m*, *R* 3*m*. In the next step, structure solution was initiated in all possible space groups using the parallel tempering algorithm of the FOX programme [16] starting from Ca, and Zr atoms and rigid PO_4 tetrahedra as building blocks. The best reliability factors were found for the space group *R*32. The resulting model has been further checked with the ADDSYM routine from the PLATON programme [17]. There were no indications for a hidden higher symmetry.

Following structure solution, the model was refined by the Rietveld method using the FULLPROF.2000 programme [18]. The background was modelled by a set of consecutive points with refineable intensities. Common isotropic displacement factors were refined for each position. For the allocation of Mn to specific cation sites of Ca, Zr1 and Zr2, constrained refinement of occupation factor were performed. The sum of two occupation factors (Mn and Zr or Mn and Ca) was fixed to 1, but individual values were refined. The result of calculation indicated that Mn atoms share Zr1 site 49(Mn):51(Zr)%. The refinement of both Zr sites with fixed mixed occupations of Mn and Zr was performed as well in order to check the possibility that Mn atoms can be distributed between both sites, but this led to worse reliability factors. In the following refinement occupation factors were fixed to calculated value.

Incorporation of Mn atoms into Zr position led to the split of the site (two 6*c* sites instead of one 12*c* in NZP archetype) and, as following, to vanishing of *c* glide plane. The refinement converged at $R_B = 3.36\%$, $R_f = 3.98\%$, $R_p = 4.72\%$, $R_{wp} = 5.94\%$, $\chi^2 = 1.4$ (not corrected for background). Cell parameters and details of the data collection, a list of atomic parameters as well as selected distances can be found in Tables 1 3, respectively. Observed and calculated XRD patterns are shown in Fig. 1a. Small reflections belonging to HT modification (3.8 wt%) were found and taken into account during calculations.

$CaMn_{0.5}Zr_{1.5}(PO_4)_3$ (or $Ca_{2/3}Mn_{1/3}Zr(PO_4)_2$) phosphate synthesized at 900 °C (HT phase) was indexed using the TOPAS software package in an orthorhombic cell ($6.23 \times 6.62 \times 14.47$ Å^3). Initially, an attempt to use the structure of $CaZr(PO_4)_2$ (space group P_{212121}) [19] as an analogue was made. However, a closer look at the reported fractional coordinates indicated that the structure has been described in an unnecessarily low symmetry. This observation was confirmed when the structure was checked using the MISSYM algorithm implemented in the Platon programme: within a few standard uncertainties the P_{212121} model fulfills the symmetry requirements of the centrosymmetric space group *Pnma*.

Table 1
Crystallographic data for LT phase and HT phase of $CaMn_{0.5}Zr_{1.5}(PO_4)_3$.

	LT phase	HT phase
Chemical formula	$CaMn_{0.5}Zr_{1.5}(PO_4)_3$[a]	$Ca_{0.66}Mn_{0.33}Zr(PO_4)_2$[b]
Crystal system, *space group*	*trigonal, R32 (no. 155)*	*orthorhombic, Pnma (no. 62)*
a, Å	8.7850(2)	6.2350(3)
b, Å	8.7850 (2)	6.6281(3)
c, Å	22.6496(3)	14.4731(6)
V, Å^3	1514.8(1)	598.13(5)
Z	6	4
$T_{synthesis}$ /$T_{data\ collection}$, °C	700 / 25	900 / 25
M (g/mol)	489.297	251.643
λ, Å	1.54059	1.54059
R_b, %	3.36	5.90
R_{wp},%	5.94	11.4

[a] R_f 3.98%, R_p 4.72%, R_{exp} 4.82%, χ^2 1.41.
[b] R_f 4.62%, R_p 8.46%, R_{wp} 11.40%, χ^2 1.40.

Table 2
Structural XRPD data and details of the structure refinement for the LT modification of $CaMn_{0.5}Zr_{1.5}(PO_4)_3$.

Atom	LT phase					
	Site	*x/a*	*y/b*	*z/c*	*occ.*	B_{iso}
Ca	6c	0	0	0.2468(4)	1.0	3.5(1)
Zr1	6c	0	0	0.8930(1)	0.5	1.2(2)
Mn1	6c	0	0	0.8930(1)	0.5	1.2(2)
Zr2	6c	0	0	0.4011(1)	1.0	2.4(2)
P1	9f	0.2901(2)	0	0	1.0	2.0(5)
P2	9f	0.7054(4)	0	1/2	1.0	1.8(5)
O1	18f	0.1634(5)	−0.0298(6)	−0.0508(1)	1.0	1.5(5)
O2	18f	0.2896(8)	−0.1725(7)	0.0113(2)	1.0	2.5(5)
O3	18f	0.7921(6)	0.0137(7)	0.5622(2)	1.0	2.3(5)
O4	18f	0.5273(6)	−0.1540(6)	0.4972(2)	1.0	1.2(3)

[a]Trigonal, *R32* (155), *Z* 6, *a* 8.7850(2) Å, *c* 22.6496(7) Å, *V* 1514.8(1) Å^3, esd's in parentheses.

In order to obtain an unbiased starting model the crystal structure of the high temperature polymorph was solved from scratch using a global optimization programme FOX, following the same procedure as for low temperature modification. Subsequently, the structure was refined by the Rietveld method using FullProf.2000. During the calculations trials to substitute Ca and Zr sites with Mn were performed and the occupancy ratio was refined in the same way as for the LT modification. Successful refinement was obtained for Mn atoms sharing one position of calcium (4*c*) with ratio 66:33%. The refinement converged at R_B =5.90%, R_f=4.62%, R_p=8.46%, R_{wp}=11.40%, χ^2=1.4 (not corrected for background). A small impurity (2.66 wt%) of remaining LT modification was found during the refinement. Details of the data collection and cell parameters are given in Table 1, list of atomic parameters in Table 4 and selected distances in Table 3, respectively. Observed and calculated XRD patterns are shown in Fig. 1b.

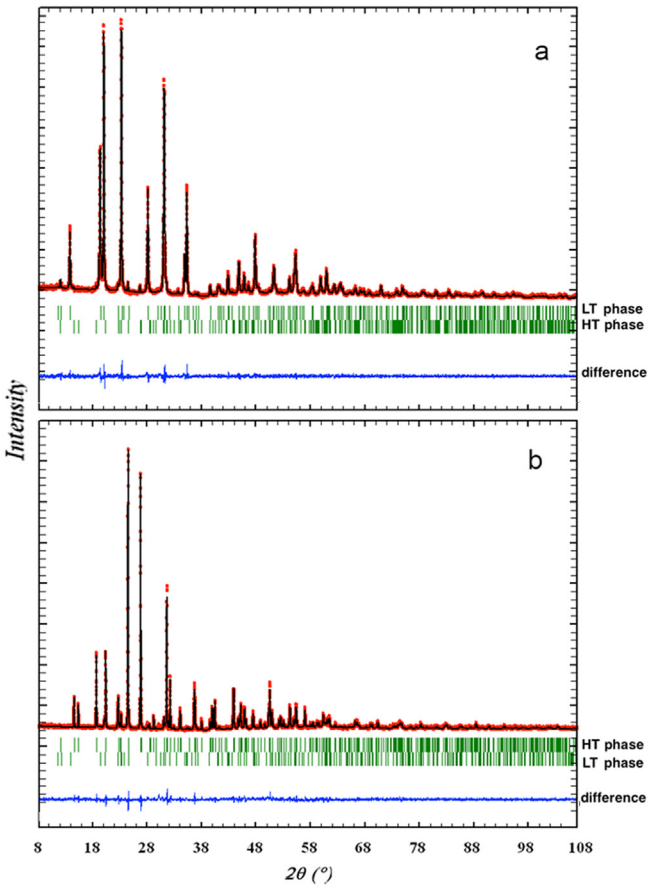

Fig. 1. Observed (points) and calculated (line) XRPD pattern for $CaMn_{0.5}Zr_{1.5}(PO_4)_3$: (a) the LT phase of (96.2 wt%) with minor amounts of HT phase (3.8 wt%), (b) the HT phase (97.3 wt%) with minor amounts of LT phase (2.66 wt%). Vertical bars indicate the positions of the Bragg peaks; the difference pattern is represented at the bottom; CuK*a* radiation, *λ* 1.540593 Å, *T* 25 °C, STOE STADI MP diffractometer, 2*θ* range 8–110°, step size 0.009°, data collection time ~16 h.

2.7. Raman analysis

From the selection rules of factor group D_3 (space group *R*32) a total number of 72 vibrational modes are predicted for the trigonal $CaMn_{0.5}Zr_{1.5}(PO_4)_3$ with the irreducible representations $\Gamma = 17A_1 + 19A_2 + 36E$. These calculations on the trigonal unit cell show that 52 modes ($17A_1 + 35E$) are Raman active while 53 modes ($18A_2 + 35E$) are IR active; two modes are acoustic ($A_2 + E$).

Table 3
Selected interatomic distances (Å) and angles (°) in the crystal structure of the LT modification of $CaMn_{0.5}Zr_{1.5}(PO_4)_3$.

Distance, Å			Angle, °		Angle, °	
Ca1	O4	2.406(8)*3	O1–Zr1|Mn1–O1	84.9(4)*3	O2–P1–O2	121.2(2)
Ca1	O2	2.757(9)*3	O1–Zr1|Mn1–O4	98.7(3)*3	O2–P1–O1	108.1(2)*2
Zr1|Mn1	O1	2.026(5)*3	O1–Zr1|Mn1–O4	94.2(3)*3	O2–P1–O1	108.3(2)*2
Zr1|Mn1	O4	2.169(4)*3	O4–Zr1|Mn1–O4	82.3(3) *3	O1–P1–O1	100.4(2)
Zr2	O3	2.068(6)*3	O3–Zr2–O3	104.9(4)*3	O4–P2–O3	110.8(2)*2
Zr2	O2	2.076(6)*3	O2–Zr2–O3	89.1(4)*3	O4–P2–O4	105.5(2)
P1	O2	1.532(4)	O2–Zr2–O3	78.3(4)*3	O4–P2–O3	100.4(2)*2
P1	O1	1.536(4)	O2–Ca1–O2	104.6(2)*3	O3–P2–O3	127.1(3)
P2	O4	1.472(5)	O2–Ca1–O4	109.7(2)*3		
P2	O3	1.567(2)	O4–Ca1–O4	115.6(2)*3		
			O2–Ca1–O2	62.0(3) *3		

Table 4
Structural XRPD data and details of the structure refinement for the HT modification of $Ca_{0.66}Mn_{0.33}Zr(PO_4)_2$.

Atom	HT phase					
	Site	*x/a*	*y/b*	*z/c*	*occ.*	B_{iso}
Ca	4*c*	0.5550(4)	3/4	0.1524 (2)	0.66(2)	3.2(2)
Mn	4*c*	0.5550(4)	3/4	0.1524(2)	0.33(2)	2.7(1)
Zr1	4*c*	0.8268(2)	1/4	0.1102(1)	1.0	1.9(4)
P1	4*c*	0.5486(3)	3/4	0.3823(5)	1.0	2.0(8)
P2	4*c*	0.3748(3)	1/4	0.1484(3)	1.0	2.2(8)
O1	4*c*	0.1669(8)	1/4	0.0951(3)	1.0	2.9(8)
O2	8*d*	0.5185(4)	0.4255(4)	0.1196(2)	1.0	2.3(8)
O3	4*c*	0.3262(8)	¼	0.2509(3)	1.0	1.5(8)
O4	4*c*	0.6766(9)	¾	0.2970(3)	1.0	2.3(8)
O5	4*c*	0.3953(4)	0.9265(4)	0.3872(3)	1.0	2.1(8)
O6	8*d*	0.7004(7)	3/4	0.4635(3)	1.0	1.5(8)

[a] orthorhombic, P*nma* (62), *Z* 4, *a* 6.2350(3) Å, *b* 6.6281(3) Å, *c* 14.4731(6) Å, *V* 598.13(5) Å^3, esd's in parentheses.

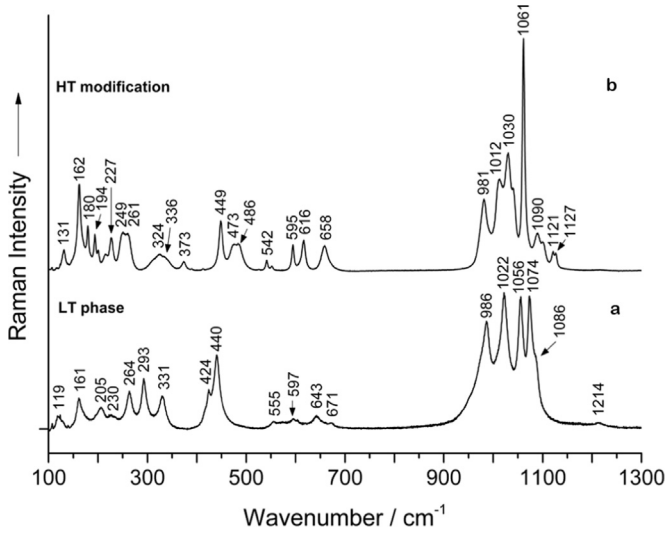

Fig. 2. Raman spectra of polycrystalline $CaMn_{0.5}Zr_{1.5}(PO_4)_3$ in the region between 100 and 1300 cm ^{1}: (a) low temperature modification and (b) high temperature modification.

On the other hand a total number of 144 vibrational modes are predicted for the orthorhombic $Ca_{0.66}Mn_{0.33}Zr(PO_4)_2$ (factor group D_{2h}, space group *Pnma*) with the irreducible representations $\Gamma = 22A_g + 14A_u + 14B_{1g} + 22B_{1u} + 22B_{2g} + 14B_{2u} + 14B_{3g} + 22B_{3u}$. In this case 72 modes ($22A_g + 14B_{1g} + 22B_{2g} + 14B_{3g}$) are Raman active while 55 modes are IR active ($21B_{1u} + 13B_{2u} + 21B_{3u}$); three modes are acoustic ($B_{1u} + B_{2u} + B_{3u}$). The Raman spectrum of the trigonal $CaMn_{0.5}Zr_{1.5}(PO_4)_3$ exhibits less visible Raman modes than the Raman spectrum of the orthorhombic high temperature phase because of the high number of doubly degenerated vibrational modes (E type). The Raman spectrum of polycrystalline $CaMn_{0.5}Zr_{1.5}(PO_4)_3$ (Fig. 2a, S1 2 (Supporting information)) shows Raman modes with high intensities at 1074, 1056, 1022, 986, 440 cm ^{1}, medium modes at 1086, 424, 331, 293, 264, 161 cm ^{1} and weak modes at 1214, 1174, 964, 671, 643, 597, 572, 555, 449, 416, 302, 230, 205, 170, 139, 128, 124, 119, 107 cm ^{1} (Table 5).

On the other hand the Raman spectrum of the high temperature modification (Fig. 2b) exhibits strong vibrational modes at 1061(vs), 1042, 1030, 1012, 981, 449, 162 cm ^{1}, medium bands at 1090, 658, 616, 595, 486, 473, 261, 249, 227, 194, 180, 131 cm ^{1} and weak modes at 1127, 1121, 1102, 1065, 986, 664, 552, 542, 412, 390, 373, 336, 324, 316, 214, 201, 172, 154, 107 cm ^{1}. Because of the partially overlapping Raman bands, not all of the calculated vibrational modes can be resolved experimentally. Because of the high bond strength and force constants of the P O bonds (P O distances ranging from 1.472 Å and 1.567 Å), P O stretching vibrations can be observed in the high wavenumber region. All Raman spectra of phosphates exhibit internal vibrational modes between 900 and 1200 cm ^{1} corresponding to the symmetric (ν_1) and asymmetric (ν_3) P O stretching vibrations of the PO_4 tetrahedra. Internal modes involve atomic vibrations of the complex ionic groups that leave their centre of mass stationary; on the other hand external vibrational modes are related to complex ionic groups that vibrate as rigid units [20]. Symmetric and asymmetric O P O bending vibrations (ν_s and ν_4) occur in the wavenumber region between 400 and 680 cm ^{1}. Raman bands below 400 cm ^{1} are caused mainly by complex vibrations involving the metal atoms (M=Ca^{2+}, Mn^{2+}, Zr^{4+}) and rotational modes of the PO_4 units at the very low frequency region (external modes).

In situ high temperature Raman spectra reveals that phase transition takes place in the range from 800 to 875 °C (Fig. 3). The most noticeable changes occur in the wavenumber range 220 400 cm ^{1}, 550 750 cm ^{1} and between 900 and 1100 cm ^{1}.

3. Results and discussion

Despite the different space groups (*R*32 instead of *R* 3*c*), the crystal structure of the low temperature polymorph still retains the main features of the *NZP* type structure. The Mn atoms share the framework site Zr1 (Wyckoff position 6*c*) with a site

Table 5
Selected interatomic distances (Å) in the crystal structure for HT modification of $Ca_{0.66}Mn_{0.33}Zr(PO_4)_2$.

Distance, Å		Angle, °		Angle, °	
CaMn O2	2.213(4)*2	O2–CaMn–O2	152.31(16)	O4–P1–O5	112.9(2)*2
CaMn O4	2.226(8)	O2–CaMn–O4	103.64(14)*2	O4–P1–O6	108.1(6)
CaMn O4	2.470(6)	O2–CaMn–O4	87.73(14)*2	O5–P1–O5	101.3(2)
CaMn O5	2.490(5)*2	O2–CaMn–O5	119.97(17)*2	O5–P1–O6	110.8(2)*2
CaMn O6	2.777(8)	O2–CaMn–O5	65.46(18)*2	O3–P2–O1	109.9(5)
Zr O3	2.008(10)	O2–CaMn–O6	77.63(14)*2	O3–P2–O2	112.7(2)*2
Zr O6	2.128(8)	O4–CaMn–O4	92.5(2)	O1–P2–O2	111.2(2)*2
Zr O1	2.130(10)	O4–CaMn–O5	86.97(15)*2	O2–P2–O2	99.3(2)
Zr O5	2.186(5)*2	O4–CaMn–O5	151.83(11)*2		
Zr O2	2.252(5)*2	O4–CaMn–O6	53.9(2)		
P1 O4	1.453(10)	O5–CaMn–O6	122.92(11)*2		
P1 O5	1.514(5)*2	O5–CaMn–O5	56.20(16)		
P1 O6	1.514(10)	O4–CaMn–O6	146.5(2)		
P2 O3	1.512(11)				
P2 O1	1.513(10)				
P2 O2	1.521(5)*2				

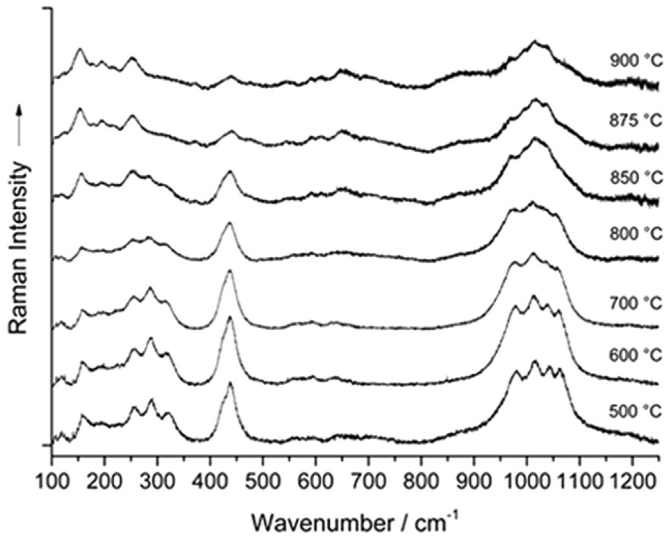

Fig. 3. *In situ* high temperature Raman spectra of $CaMn_{0.5}Zr_{1.5}(PO_4)_3$ measured in the range from 500 up to 900 °C.

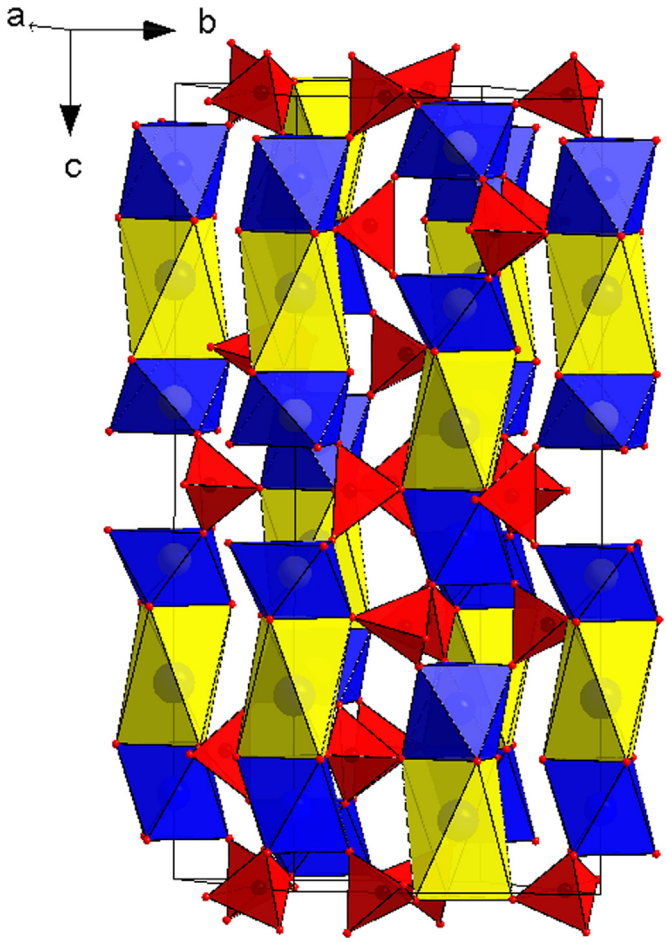

Fig. 4. Structure of trigonal LT modification of $CaMn_{0.5}Zr_{1.5}(PO_4)_3$.

Table 6
Selected average interatomic distances (Å) in the crystal structures of LT and HT phase of $CaMn_{0.5}Zr_{1.5}(PO_4)_3$ (present work), $Ca_{0.5}Zr_2(PO4)_3$ [21] and $Mn_{0.5}Zr_2(PO_4)_3$ [9].

$CaMn_{0.5}Zr_{1.5}(PO_4)$ (LT)		$CaMn_{0.5}Zr_{1.5}(PO_4)$ (HT)		$Ca_{0.5}Zr_2(PO_4)_3$		$Mn_{0.5}Zr_2(PO_4)_3$	
Ca–O, *av*	2.587 Å	Ca/Mn–O, av	2.417 Å	Ca–O, *av*	2.49 Å	Mn–O, *av*	2.31 Å
Zr/Mn–O, *av*	2.084 Å	Zr–O, *av*	2.159 Å	Zr–O, *av*	2.16 Å	Zr–O, *av*	2.06 Å
P–O, *av*	1.527 Å	P–O, *av*	1.508 Å	P–O, *av*	1.52 Å	P–O, *av*	1.56 Å

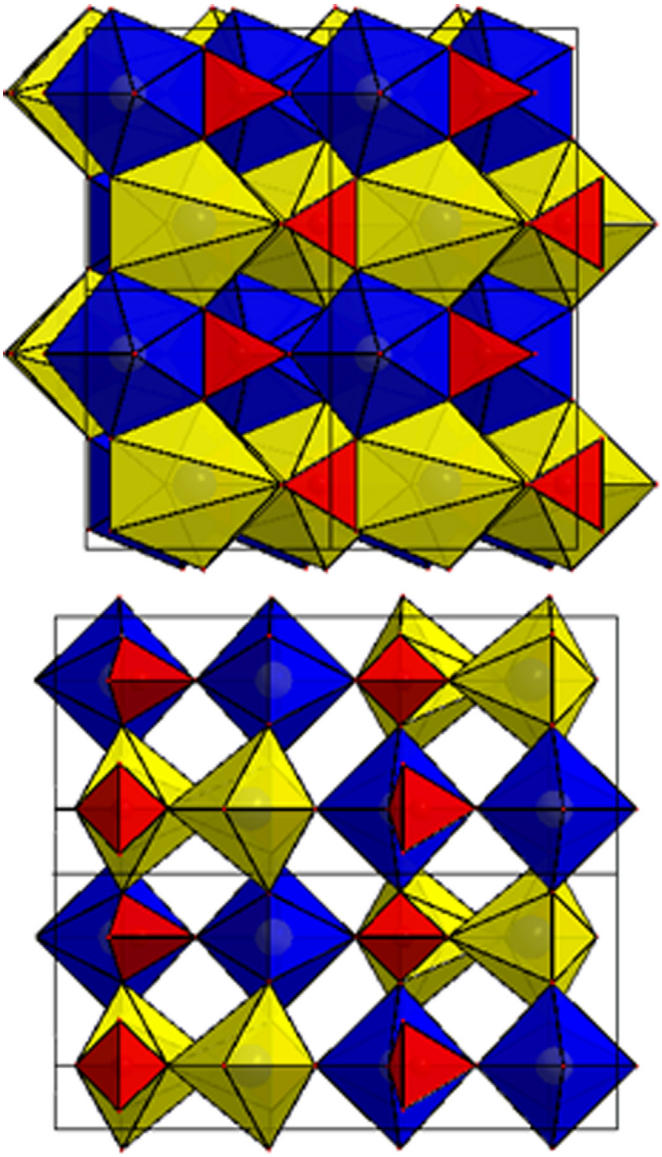

Fig. 5. The crystal structure of HT modification $CaMn_{0.5}Zr_{1.5}(PO_4)_3$ viewed along (top) [001] and (bottom) [100] directions showing the three-dimensional framework.

population of 49% for Mn and 51% for Zr. The *6c* position of Zr2 in turn is fully occupied with Zr atoms. Both Zr/Mn and Ca atoms are six fold coordinated. Ca O and Zr/Mn O bond lengths are consistent with those reported for $NaZr_2(PO_4)_3$ [1], $Ca_{0.5}Zr_2(PO_4)_3$ [21] and $Mn_{0.5}Zr_2(PO_4)_3$ [9]. Zr/Mn O_6 and PO_4 polyhedra are slightly distorted, e.g. the P O distances are in the range 1.472 1.567 Å (mean 1.527 Å) (Table 4). The structure contains a 3D framework of corner sharing Zr/MnO_6 octahedra and PO_4 tetrahedra. Ca atoms completely fill one kind of cavity in the structure. Structural

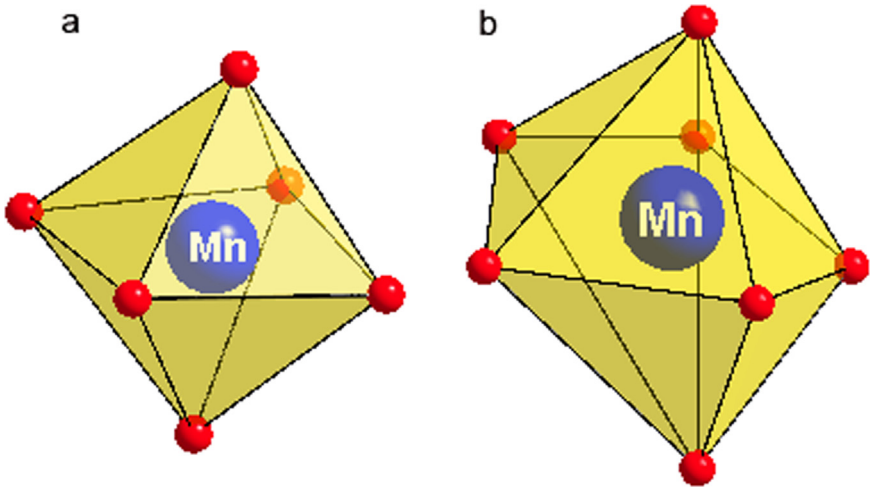

Fig. 6. Local coordination around the two different Mn atoms in the $CaMn_{0.5}Zr_{1.5}(PO_4)_3$: (a) Mn–$O_6$ octahedra of LT modification and (b) Mn–O_7 poly- hedra of HT modification.

units consisting of two octahedra and three tetrahedra are con nected to form ribbons parallel to the *c* axis. These ribbons are linked together perpendicular to the *c* direction by tetrahedra to build a three dimensional framework (Fig. 4).

Despite different space groups (*Pnma* instead of P_{212121}), the crystal structure of the orthorhombic high temperature poly morph still retains the main features of the $CaZr(PO_4)_2$ structure [21]. The Zr atom is sevenfold coordinated with a mean Zr O distance of 2.158 Å, which is comparable to that of the ZrO_7 polyhedron (2.16 Å) in dizirconium oxophosphate $Zr_2O(PO_4)_2$ [22]. Mn^{2+} cation share seven fold coordinated position *4c* with Ca^{2+} with occupancies of 33% Mn and 66% Ca. The Ca/Mn O distance (2.417 Å) is consistent with the weighted sum of their ionic radii according to Shannon [23]. PO_4 polyhedra are distorted; the P O distances are in the range 1.453 1.521 Å (mean 1.508 Å) (Table 4) which is in good agreement with the average value of 1.537 Å found in the literature for the phosphates [24]. (Table 6)

The crystal structure of the high temperature modification consists of Ca/MnO_7, ZrO_7 and PO_4 polyhedra. They share edges and form infinite chains along the *b* direction (Fig. 5a). Individual chains are linked via oxygen atoms and form two dimensional layers (Fig. 5b). These layers are linked with neighbouring sheets in the *c* direction via oxygen atoms (4 layers per unit cell) resulting in the formation of a three dimensional structure.

The rhombohedral structure of LT modification changes to an orthorhombic cell with the following change in space group from *R*32 to *Pnma*. Due to reconstructive nature of structural changes and co existence of both modification at broad temperature in terval, we conclude that compound undergoes 1st order phase transition. Mn^{2+} cations occupy different types of positions in the studied structures. In the LT phase Mn shares the framework po sition *6c* with Zr1, in the HT phase Mn shares *4c* position with Ca. Therefore, Mn coordination is changed drastically. In the LT modification it has octahedral coordination and Zr/Mn O, av is 2.097 Å, in the HT modification Mn^{2+} cations have seven fold coordination and Ca/Mn O, *av* 2.417 Å (Fig. 6).

4. Conclusions

The results of this work show that Mn^{2+} cations occupy dif ferent types of positions in low and high temperature poly morphs of $CaMn_{0.5}Zr_{1.5}(PO_4)_3$. A change in coordination number of Mn (6 for LT phase, 7 for HT phase) results in a change of Mn O bond lengths (Mn O, *av.*=2.084 Å for LT phase, Mn O, *av.*=2.417 Å for HT phase).

These structural changes provide one possible explanation for the observed significant change in optical properties. In order to better understand the mechanism of luminescence we intend to further investigate the optical properties of the studied compound in light of the structural information here presented.

Aknowlegements

We thank Volker Kahlenberg and Gilles Wallez for valuable crystallographic corrections, Roberto Nervo and Michael Reynolds for proofreading. The financial support of the Ministry of Educa tion and Science of the Russian Federation (Project no. 11.1036.2014/K) is gratefully acknowledged.

Appendix A. Supplementary material

Supplementary data associated with this article can be found in the online version at doi:10.1016/j.jssc.2015.12.014.

References

[1] L. Hagman, P. Kierkegaard, Acta Chem. Scand. 22 (1968) 1822.
[2] T. Masui, K. Koyabu, S. Tamura, N. Imanaka, J. Zhang, J. Alloy. Compd. 418 (2006) 73–76.
[3] M. Hirayama, N. Sonoyama, A. Yamada, R. Kanno., J. Solid State Chem. 182 (2009) 730–735.
[4] B. Glorieux, V. Jubera, A. Orlova, A. Kanunov, A. Garcia, C. Pallier, T. Oleneva, Inorg. Mater. 49 (1) (2013) 82–88.
[5] M.P. Saradhi, V. Pralong, U.V. Varadaraju, B. Raveau, Chem. Mater. 21 (2009) 1793–1795.
[6] I.M. Nagpure, K.N. Shinde, V. Kumar, J. Alloy. Compd. 492 (2010) 384–388.
[7] N. Semi, Solid State Ion. 181 (2010) 659–663.
[8] K. Bakhous, F. Cherkaoui, A. Nenabad, J.M. Savariault, Mater. Res. Bull. 34 (2) (1999) 263–269.
[9] A. Mouline, M. Alami, R. Brochu, R. Olazcuaga, C. Parent, G. Le Flem, Mater. Res. Bull. 35 (2000) 899–908.
[10] B. Glorieux, A. Orlova, A. Garcia, A. Kanunov, V. Jubera, "CIMTEC-2010" Book of Abstracts, (2010) 100–101.
[11] M. Orlova, B. Glorieux, A. Orlova, P. Salnikov, V. Kahlenberg, EPDIC13, Book of Abstracts, (2012) 136.
[12] M.I. Aroyo, J.M. Perez-Mato, D. Orobengoa, E. Tasci, G. Flor, A. Kirov, Bulg. Chem. Commun. 43 (2) (2011) 183–197.

[13] M.I. Aroyo, J.M. Perez-Mato, C. Capillas, E. Kroumova, S. Ivantchev, G. Madariaga, A. Kirov, H. Wondratschek, Z. Kristallogr. 221 (1) (2006) 15–27.
[14] M.I. Aroyo, A. Kirov, C. Capillas, J.M. Perez-Mato, H. Wondratschek, Acta Crystallogr. A62 (2006) 115–128.
[15] E. Kroumova, M.I. Aroyo, J.M. Perez-Mato, A. Kirov, C. Capillas, S.H. Ivantchev, Phase Transit. 76 (2003) 155–170.
[16] V. Favre-Nikolin, R. Cerny, Mater. Sci. Forum (2004) 443–444.
[17] A.L. Spec., PLATON, University of Utrecht, The Netherlands, 2006.
[18] J. Rodriguez-Carvajal, Journal of recent developments of the program FULL-PROF, in commission on powder diffraction (IUCr), Newsletter 26 (2001) 12–19.
[19] K. Fukuda, K. Fukutani, Powder Diffr. 18 (4) (2003) 296–300.
[20] P.N. de Aza, C. Santos, A. Pazo, S. de Aza, R. Cusco, L. Artús, Chem. Mater. 9 (1997) 912–915.
[21] W. Fischer, L. Singheiser, D. Basu, A. Dasgupta, Powder Diffr. 19 (2) (2004) 153–156.
[22] W. Gebert, E. Tillmanns, Acta Crystallogr. B 31 (1975) 1768–1770.
[23] R.D. Shannon, Acta Crystallogr. A32 (1976) 761–767.
[24] W.H. Baur, Acta Crystallogr. B30 (1974) 1195–1215.